

Theory and simulation of cohesive diffusion in nanopores: Transport in subcritical and supercritical regimes

Chandra Saravanan

Department of Chemistry, University of Massachusetts, Amherst, Massachusetts 01003

Scott M. Auerbach^{a)}

Departments of Chemistry and Chemical Engineering, University of Massachusetts, Amherst, Massachusetts 01003

(Received 19 January 1999; accepted 17 March 1999)

We have studied a lattice model of self-diffusion in nanopores, to explore how loading, temperature, and adsorbate coupling influence benzene self-diffusion in Na-X and Na-Y zeolites. We propose a simple method for determining how adsorbate-adsorbate interactions modify activation energies of site-to-site jumps. We apply a mean-field approximation that describes transport semiquantitatively for a wide variety of system parameters, simplifying kinetic Monte Carlo simulations. We also derive an analytical diffusion theory that provides semiquantitative apparent activation energies, and qualitatively reasonable loading dependencies. We have found that supercritical systems exhibit three characteristic loading dependencies of diffusion, depending upon the degree of degeneracy of lattice sites. Subcritical diffusion systems are dominated by cluster formation, exhibiting intriguing loading dependencies with broad regions of constant diffusivity. Our model for benzene in Na-X is in excellent qualitative agreement with pulsed field gradient nuclear magnetic resonance (NMR) diffusivities, and in qualitative disagreement with tracer zero-length column (TZLC) data. We suggest that high-temperature TZLC experiments should be performed, to test whether the coverage of maximum diffusivity decreases with increasing temperature. © 1999 American Institute of Physics. [S0021-9606(99)70422-8]

I. INTRODUCTION

The transport properties of adsorbed molecules play a central role in separations and reactions that take place within zeolites and other nanoporous solids. Significant effort has been devoted to understanding diffusion in zeolites,^{1,2} revealing fascinating physical effects such as anomalous diffusion,^{3,4} correlated cluster dynamics,⁵ soft core interactions,⁶ broken symmetry,⁷ and percolation.⁸ Despite this recent progress, developing a predictive analytical theory for normal diffusion in zeolites has remained challenging,⁹ due to the coupling between infrequent event dynamics and strong adsorbate-adsorbate interactions. To address this issue, we have developed new theory and simulation techniques for modeling self-diffusion in zeolites, based on mean-field dynamics of cage-to-cage motion. In this article, we elaborate on a previously published letter,¹⁰ showing that excellent qualitative agreement is obtained comparing our new theory to kinetic Monte Carlo (KMC) simulations.

We apply our new theory and simulation techniques to study benzene self-diffusion in the faujasite-type zeolites, Na-X and Na-Y. Several studies have been reported on these systems, involving thermochemistry,¹¹⁻¹³ diffusion,¹⁴⁻¹⁶ crystallography,^{17,18} modeling,^{10,19-26} and NMR,^{20,23} because of persistent, qualitative discrepancies between different experimental probes of the coverage depen-

dence of self-diffusion.¹ Pulsed-field gradient (PFG) NMR diffusivities decrease monotonically with loading,¹⁴ while tracer zero-length column (TZLC) data *increase* monotonically with loading.¹⁵ TZLC is a flow method that measures the desorption rate arising from tracer exchange in a zero-length chromatographic column containing zeolite particles. The TZLC data are converted to self-diffusivities through a model assuming that tracer exchange introduces no chemical potential gradient. PFG NMR differs from TZLC in that the NMR experiment directly measures the mean square displacement of magnetically labeled particles at equilibrium in a zeolite. Addressing the discrepancy between PFG NMR and TZLC with theory and simulation will provide deep understanding of the microscopic physics essential to these transport phenomena.

Our model for benzene diffusion assumes that benzene molecules jump among S_{II} and W sites, located near Na^+ ions in supercages, and in 12-ring windows separating adjacent supercages, respectively. While this lattice of sites enables realistic modeling of benzene in faujasite, it also provides a generic platform for exploring the following effects: adsorption site inhomogeneity, repulsive adsorbate-adsorbate interactions via site blocking, and attractive adsorbate-adsorbate interactions via nearest-neighbor coupling. Indeed, we find that this lattice model portrays a rich variety of adsorption and diffusion phenomena. By varying fundamental energy scales, this system exhibits four of the five loading dependencies of self-diffusion reported by Kärger and Pfeifer,²⁷ and also supports phase transitions

^{a)}Author to whom correspondence should be addressed. Electronic mail: auerbach@chem.umass.edu

from low to high adsorbate density, analogous to vapor–liquid equilibrium of the bulk fluid.²⁸ Below, we develop generic rules governing how fundamental input parameters control the loading dependence of diffusion. We find that understanding the thermodynamics of confined fluids can be crucial for elucidating the transport properties of molecules in zeolites.

Despite the simplicity of the present lattice model (*vide infra*), this many-body diffusion problem remains challenging because of the long simulation times, and the large number of distinct, fundamental rate coefficients required by KMC. To calculate rate coefficients, we develop a simple and qualitatively reliable method that describes how adsorbate–adsorbate interactions modify activation energies of site-to-site jumps, called the parabolic jump model. To reduce simulation times, we apply a mean-field approximation^{6,29–31} (MFA) yielding $D(\theta) \equiv (1/6)k_\theta a_\theta^2$, where θ is the fractional loading, a_θ is the KMC calculated mean intercage jump length ($a_\theta \approx 11 \text{ \AA}$), and $1/k_\theta$ is the KMC calculated mean cage residence time. We also derive an analytical mean-field theory (MFT) for k_θ in the grand canonical ensemble. By comparing diffusivities obtained from these different methods, we learn what levels of theory and simulation are required to capture the loading and temperature dependence of diffusion.

We find below that MFA describes transport semiquantitatively for a wide variety of system parameters, while MFT gives semiquantitative apparent activation energies and qualitatively reasonable loading dependencies. We also find that supercritical systems exhibit three characteristic loading dependencies of diffusion, while subcritical systems are dominated by cluster formation, with broad regions of constant diffusivity. Our model for benzene in Na–X is in excellent qualitative agreement with pulsed-field gradient NMR diffusivities, and in qualitative disagreement with tracer zero-length column (TZLC) data. We suggest that high-temperature TZLC experiments should be performed, to test whether the coverage of maximum diffusivity decreases with increasing temperature. We hope these findings will enable the eventual convergence of modeling and experiment, enhancing our understanding of molecules in nanopores.

The remainder of this paper is organized as follows: in Sec. II we present our general lattice model, in Sec. III we derive our diffusion theory, and in Sec. IV we describe the simulation methodology. In Sec. V we discuss our theory and simulation results in the context of subcritical and supercritical transport, and also compare our results with experiment. Finally, in Sec. VI, we summarize our findings, and discuss prospects for future work.

II. GENERAL MODEL

We model benzene self-diffusion in Na–X and Na–Y by replacing the zeolite framework with a three-dimensional lattice of binding sites. Such a lattice model reproduces diffusive behavior accurately when site residence times are much longer than travel times between sites,^{32–34} which is the case for benzene in Na–X and Na–Y because of the strong cage–quadrupole interaction between Na and benzene.

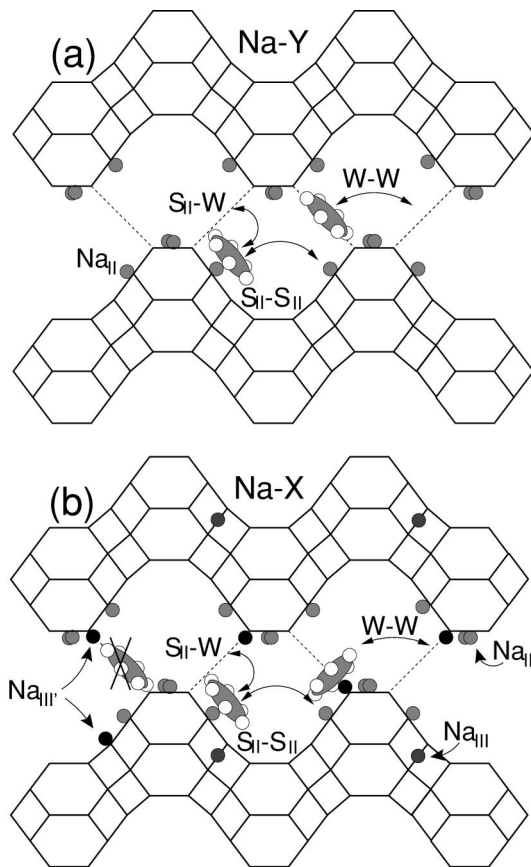


FIG. 1. Sorption sites and jumps for benzene in (a) Na–Y and (b) Na–X.

Benzene has two predominant sites in Na–Y,¹⁷ shown schematically in Fig. 1(a). In the primary site, denoted as S_{II} , benzene is facially coordinated to a supercage 6-ring, ca. 2.7 \AA above Na(II). In the secondary site, denoted as W , benzene lies in the plane of the 12-ring window separating adjacent supercages, ca. 5.3 \AA from the S_{II} site.

Locating benzene adsorption sites in Na–X is more difficult because of the influence of additional Na cations in low-symmetry positions, denoted sites III and III'. Recent crystallographic studies^{18,35} favor the prevalence of Na(III'), which lies in the 12-ring window as shown in Fig. 1(b). Na(III') cations would preclude benzene from lying in the plane of the Na–X 12-ring window. Indeed, the powder neutron diffraction study of Vitale *et al.*¹⁸ found benzene in Na–X only at S_{II} , but located only half the adsorbed benzene, suggesting that low-symmetry benzene sites near Na(III') are likely. These binding sites would act as intermediates for cage-to-cage motion, in analogy with Na–Y W sites. As such, we denote benzene sites near Na(III') cations as Na–X W sites, although strictly speaking their geometries and energies differ from those of Na–Y W sites. The lattice of benzene binding sites in Na–X and Na–Y thus contains four tetrahedrally arranged S_{II} sites and four tetrahedrally arranged, doubly shared W sites per supercage. Saturation coverages of ca. 6 molecules per cage are found for benzene in Na–X and Na–Y,¹¹ corresponding to occupation of all S_{II} and W sites. In the equations that follow, the W and S_{II} sites are denoted sites 1 and 2, respectively.

TABLE I. Activation energies and prefactors for benzene jumps in Na–X and Na–Y.

	Activation Energy (eV)		Arrhenius prefactor (s^{-1})	
	Na–Y	Na–X	Na–Y	Na–X
$S_{II} \rightarrow S_{II}$	0.25	0.15	0.8×10^{13}	0.8×10^{13}
$S_{II} \rightarrow W$	0.38	0.25	0.8×10^{13}	0.8×10^{13}
$W \rightarrow S_{II}$	0.13	0.10	1.1×10^{12}	1.1×10^{12}
$W \rightarrow W$	0.13	0.10	2.4×10^{11}	2.4×10^{11}

A lattice gas model is used to describe the thermodynamics of these systems, limiting the range of adsorbate–adsorbate interactions to nearest neighbors. The Hamiltonian for a lattice with M_1 W sites and $M_2 = 2M_1 = M - M_1$ S_{II} sites, takes the form

$$H(\vec{s}, \vec{\sigma}) = \sum_{i=1}^{M_1} s_i f_1 + \frac{1}{2} \sum_{i,j=1}^{M_1} s_i J_{ij}^{11} s_j + \sum_{i=1}^{M_1} \sum_{j=1}^{M_2} s_i J_{ij}^{12} \sigma_j + \frac{1}{2} \sum_{i,j=1}^{M_2} \sigma_i J_{ij}^{22} \sigma_j + \sum_{i=1}^{M_2} \sigma_i f_2, \quad (2.1)$$

where \vec{s} and $\vec{\sigma}$ are site occupation numbers for W and S_{II} sites, respectively, and f_1 and f_2 are their respective site free energies given by $f_i = \varepsilon_i - T s_i$. In Eq. (2.1), J_{ij}^{11} , J_{ij}^{12} , and J_{ij}^{22} are the nearest-neighbor W – W , W – S_{II} , and S_{II} – S_{II} interactions, respectively, i.e., $J_{ij}^{11} = J_{11}$ for nearest-neighbor W sites and zero otherwise, and so on for J_{ij}^{12} and J_{ij}^{22} . The site binding energies are taken as $\varepsilon_2 = -0.78$ eV and $\varepsilon_1 = -0.63$ eV for benzene in Na–X,¹⁰ and $\varepsilon_2 = -0.78$ eV and $\varepsilon_1 = -0.53$ eV for benzene in Na–Y.⁶ Site 2 is chosen for the zero of entropy in both Na–X and Na–Y, giving $s_2 \equiv 0$.

The infinite dilution site-to-site jump activation energies and Arrhenius prefactors used in this study are given in Table I. The activation energies are extracted from experimental data for benzene in Na–X^{14,23} and Na–Y,^{23,36} which broadly agree with various simulation results.^{23–25,37} The Arrhenius prefactors are calculated from transition state theory with dynamical corrections for benzene in Na–Y,²⁶ and are assumed to hold also for benzene in Na–X. Using the Arrhenius prefactors in Table I, and the fact that $s_1 = k_B \ln(\nu_{2 \rightarrow 1} / \nu_{1 \rightarrow 2})$ where k_B is Boltzmann's constant, we find that $s_1 = 1.98 k_B = 0.00017$ eV/K for benzene in Na–X and Na–Y. This entropy difference increases the W site population by a factor of ca. 7 at infinite dilution, more than compensating for the fact that there are twice as many S_{II}

sites as W sites. The data in Table I are also used to determine the infinite dilution jump rates for benzene in Na–X¹⁰ and Na–Y^{6,36} at any temperature T , according to $k_{i \rightarrow j} = \nu_{i \rightarrow j} e^{-\beta E_a(i \rightarrow j)}$, where $\beta = (k_B T)^{-1}$.

The adsorbate–adsorbate parameters, J_{ij} , are obtained from the second virial coefficient of the heat of adsorption,^{11,12} yielding ca. $J = J_{12} = J_{22} \cong -0.03$ eV. J_{11} is set to zero because the W – W intracage distance is larger than typical S_{II} – S_{II} and W – S_{II} intracage distances, i.e., $d(S_{II}, S_{II}) \approx d(S_{II}, W) \approx 5$ Å, while $d(W, W) \approx 9$ Å.¹⁷ However, to determine qualitatively how adsorbate–adsorbate interactions control the loading dependence of the self-diffusivity, we vary J_{12} and J_{22} over the range 0 to -0.10 eV.

The attractive adsorbate–adsorbate interactions introduce new complexities into the kinetics of the diffusion problem. An extreme case of this was recently reported by Sholl and Fichthorn,⁵ wherein strong adsorbate–adsorbate interactions generated transport dominated by correlated cluster dynamics instead of single molecule jumps. While such correlated clusters are not likely to dominate benzene diffusion in faujasite, adsorbate–adsorbate interactions will modify jump activation energies for site-to-site rate coefficients, depending upon specific configurations of neighboring adsorbates. In order to account for this, we have generalized a model that relates binding energies to transition state energies used previously by Hood *et al.*,³⁸ and also used by us for predicting mobilities in zeolites.²³ To implement this approach for benzene in faujasite, it is convenient to write the lattice gas Hamiltonian in the following form:

$$H(\vec{n}) = \sum_{i=1}^M n_i \tilde{f}_i + \frac{1}{2} \sum_{i,j=1}^M n_i \tilde{J}_{ij} n_j, \quad (2.2)$$

where $\vec{n} = (n_1, n_2, \dots, n_M)$ are site occupation numbers listing a configuration of the system, and $\tilde{f}_i = \varepsilon_i - T s_i$ is the free energy for binding in site i . In Eq. (2.2), \tilde{J}_{ij} is the nearest-neighbor interaction between sites i and j , i.e., $\tilde{J}_{ij} = 0$ if sites i and j are not nearest neighbors.

We assume that the minimum energy hopping path connecting adjacent sorption sites is characterized by intersecting parabolas, shown in Fig. 2, with the site-to-site transition state located at the intersection point. For a jump from site i to site j , with $i, j = 1, \dots, M$, the hopping activation energy including adsorbate–adsorbate interactions is given by

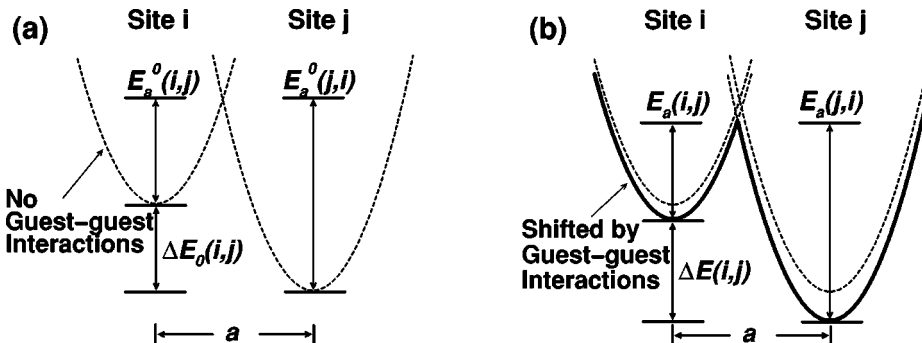


FIG. 2. Site-to-site jump activation energies (a) without and (b) with effect of guest–guest interactions, approximated with parabolic jump model.

$$E_a(i,j) = E_a^{(0)}(i,j) + \Delta E_{ij} \left(\frac{1}{2} + \frac{\delta E_{ij}^{(0)}}{k_{ij} a_{ij}^2} \right) + \Delta E_{ij}^2 \left(\frac{1}{2k_{ij} a_{ij}^2} \right), \quad (2.3)$$

where $E_a^{(0)}(i,j)$ is the activation energy without adsorbate–adsorbate interactions, i.e., the infinite dilution activation energy, and a_{ij} is the jump distance. ΔE_{ij} is the *shift* in the energy difference between sites i and j resulting from adsorbate–adsorbate interactions, and is given by $\Delta E_{ij} = \delta E_{ij} - \delta E_{ij}^{(0)} = (E_j - E_i) - (\bar{\epsilon}_j - \bar{\epsilon}_i)$, where $E_k = \bar{\epsilon}_k + \sum_{l=1}^M \tilde{J}_{kl} n_l$ for a particular lattice configuration \vec{n} . In Eq. (2.3), the harmonic force constant k_{ij} is defined for each distinct jump (independent of direction), and is given by

$$k_{ij} = \left(\frac{2}{a_{ij}} \right)^2 \left[\frac{1}{2} (E_a^{(0)}(i,j) + E_a^{(0)}(j,i)) + \sqrt{E_a^{(0)}(i,j) \cdot E_a^{(0)}(j,i)} \right]. \quad (2.4)$$

This method allows the rapid estimation of configuration-dependent barriers during a kinetic Monte Carlo (KMC) simulation, knowing only infinite dilution barriers and the nearest-neighbor interactions defined above. The details of the simulation will be discussed in Sec. IV. The parabolic jump model (PJM) is most accurate when the spatial paths of jumping molecules are not drastically changed by adsorbate–adsorbate interactions, although the energies can change as shown in Fig. 2. We have performed several many-body reactive-flux correlation function calculations³⁹ that give barriers in qualitative agreement with the parabolic jump model. A more detailed test of this method will be reported in a forthcoming publication.⁴⁰

III. ANALYTICAL THEORY

As stated in the last section, we model benzene diffusion through faujasite as consisting of activated adsorbate jumps among S_{II} and W binding sites. We can simplify this conceptually and computationally, by imagining that long-range motion involves jumps from one “cage site” to an adjacent cage site.^{41,42} As such, a random walk through faujasite reduces to hopping on the tetrahedral lattice of supercages. As stated in the Introduction, we have previously shown that a mean field analysis applied to this cage-to-cage motion yields $D(\theta) \cong \frac{1}{6} k_{\theta} a_{\theta}^2$, where θ is the fractional loading, a_{θ} is the mean intercage jump length ($a_{\theta} \cong 11 \text{ \AA}$), and $1/k_{\theta}$ is the mean cage residence time.⁶ Computing $D(\theta)$ generally requires mean square displacement (MSD) calculations, which formally scale as $N_S \cdot (1 + N_t)$, where N_S is the number of simulation steps and N_t is the number of MSD time bins. On the other hand, calculating k_{θ} and a_{θ} formally scales as N_S , since these are time independent quantities. Since N_t is usually of order 10–100, our mean field approximation can offer significant computational speedups over brute force MSD calculations.

This mean field approximation also serves as the launching point for our analytical diffusion theory. We have previously shown⁶ that the cage-to-cage rate coefficient, k_{θ} , is given by $k_{\theta} = \kappa \cdot k_1 \cdot P_1$, where P_1 is the probability of occupying a W site, k_1 is the total rate of leaving a W site, and κ

is the transmission coefficient for cage-to-cage motion. This theory provides a picture of cage-to-cage motion involving transition state theory ($k_1 \cdot P_1$) with dynamical corrections (κ), which is valid for both weak *and* relatively strong adsorbate–adsorbate interactions. For consistency with our mean field analysis, we assume that $\kappa = \frac{1}{2}$ for all loadings. We also expect that P_1 will increase with loading, and that k_1 will decrease with loading. In this section, we derive analytical expressions for k_1 and P_1 , to elucidate how the balance between k_1 and P_1 controls the loading dependence of self-diffusion. By assuming that $a_{\theta} \cong 11 \text{ \AA}$, we arrive at a completely analytical mean field theory (MFT) for the temperature and loading dependence of the diffusion coefficient.

The loading dependence of P_1 , the probability of occupying a W site, is influenced by blocking stable S_{II} sites and by adsorbate–adsorbate interactions that modify the relative stabilities of adsorption sites. In the Na-X and Na-Y lattices, with twice as many S_{II} sites as W sites, P_1 is given by $1/(1 + 2\theta_2/\theta_1)$, where θ_1 and θ_2 are the fractional coverages on W and S_{II} sites, respectively. We determine this loading dependence from mean field theory in the grand canonical ensemble, by averaging over local fluctuations in the instantaneous energy of each adsorption site. For example, the average energy of a molecule at an S_{II} site is $f_2 + 3(J_{22}\theta_2 + J_{12}\theta_1)$, where the factor of 3 counts the number of nearest S_{II} and W sites for each S_{II} site. The occupancies in W and S_{II} sites are then Boltzmann averaged using these energies to determine θ_1 and θ_2 ,³⁹ according to

$$\theta_1 \cong \langle s_i \rangle_{MF} = \frac{e^{-\beta[(f_1 - \mu) + 6(J_{11}\theta_1 + J_{12}\theta_2)]}}{1 + e^{-\beta[(f_1 - \mu) + 6(J_{11}\theta_1 + J_{12}\theta_2)]}}, \quad (3.1)$$

$$\theta_2 \cong \langle \sigma_i \rangle_{MF} = \frac{e^{-\beta[(f_2 - \mu) + 3(J_{22}\theta_2 + J_{12}\theta_1)]}}{1 + e^{-\beta[(f_2 - \mu) + 3(J_{22}\theta_2 + J_{12}\theta_1)]}}, \quad (3.2)$$

where μ is the chemical potential. The factor of 6 in Eq. (3.1) counts the number of nearest S_{II} and W sites for each W site. We solve these simultaneous nonlinear equations for θ_1 and θ_2 self-consistently using the Newton–Raphson method.⁴³ The total fractional coverage is then given by $\theta = (\theta_1 + 2\theta_2)/3$. For comparison, we also calculate P_1 with a variable time-step KMC simulation, which we describe in the next section.

We can also derive an analytical MFT expression for the loading dependence of k_1 , the total rate of leaving a W site. The loading dependence of k_1 is determined by blocking of target sites and by adsorbate–adsorbate interactions that modify jump activation energies. A mean-field expression summarizing these effects is given by

$$k_1 \cong 6(1 - \theta_1) \langle k_{1 \rightarrow 1} \rangle + 6(1 - \theta_2) \langle k_{1 \rightarrow 2} \rangle, \quad (3.3)$$

where $6(1 - \theta_j)$ counts available target sites, and $\langle k_{1 \rightarrow j} \rangle$ averages over fluctuating rate coefficients for jumps leaving W sites. As described in the last section, we model the fluctuating activation energies according to the parabolic jump model. Assuming that fluctuations in the preexponentials can be ignored and that activation energies are Gaussian-distributed, we have that

TABLE II. Levels of theory for calculating diffusion coefficients.

Level of theory	Description
MFT	$D(\theta) = (1/6)k_\theta a_\theta^2$, $a_\theta = 11 \text{ \AA}$, k_θ from analytical theory in Sec. III
MFA	$D(\theta) = (1/6)k_\theta a_\theta^2$, a_θ , and k_θ from KMC
MSD	$D(\theta) = \lim_{t \rightarrow \infty} \langle \mathcal{R}^2(t) \rangle / 6t$ from KMC

$$\begin{aligned} \langle k_{i \rightarrow j} \rangle &\cong \nu_{i \rightarrow j} \langle e^{-\beta E_a(i,j)} \rangle \\ &= \nu_{i \rightarrow j} \cdot e^{-\beta \langle E_a(i,j) \rangle} \cdot e^{-\beta^2 \sigma_a^2(i,j)/2}, \end{aligned} \quad (3.4)$$

where $\sigma_a^2(i,j)$ is the variance of the Gaussian distribution of activation energies, i.e., $\sigma_a^2(i,j) = \langle [E_a(i,j) - \langle E_a(i,j) \rangle]^2 \rangle = \langle [E_a(i,j)]^2 \rangle - \langle E_a(i,j) \rangle^2$. We see from Eq. (2.3) that applying mean-field theory requires averages of ΔE_{ij}^k up to $k=4$. We only consider terms up to second order, since higher-order terms will typically be small. Using the notation that 1 and 2 denote nearest-neighbor W and S_{II} sites, respectively, we obtain for benzene in faujasite

$$\begin{aligned} \langle \Delta E_{11} \rangle &= 0, \\ \langle \Delta E_{12} \rangle &= (3J_{12} - 6J_{11})\theta_1 + (3J_{22} - 6J_{12})\theta_2, \\ \langle \Delta E_{11}^2 \rangle &= 8J_{11}^2\theta_1(1-\theta_1) + 8J_{12}^2\theta_2(1-\theta_2), \\ \langle \Delta E_{12}^2 \rangle &= \alpha_1\theta_1 + \alpha_2\theta_2 + \gamma_1\theta_1^2 + \gamma_2\theta_2^2 + \eta_{12}\theta_1\theta_2, \end{aligned} \quad (3.5)$$

where

$$\begin{aligned} \alpha_i &= 3J_{i2}^2 + 6J_{i1}^2 - 4J_{1i}J_{i2}, \\ \gamma_i &= 6J_{i2}^2 + 30J_{i1}^2 - 32J_{1i}J_{i2}, \\ \eta_{12} &= 18J_{12}J_{22} + 72J_{11}J_{12} - 36(J_{11}J_{22} + J_{12}^2). \end{aligned} \quad (3.6)$$

Here, we have *not* used the summation convention for adjacent indices. The numerical prefactors in Eqs. (3.5) and (3.6) arise from the site connectivity of benzene in faujasite, and are straightforwardly calculable for other host-guest systems. The second-order terms in Eq. (3.5) are typically small, suggesting that the different connectivity of S_{II} and W sites contributing to $\langle \Delta E_{12} \rangle$ is largely responsible for activation energy fluctuations in this system.

IV. KINETIC MONTE CARLO SIMULATIONS

We calculate self-diffusion coefficients for benzene in faujasite from MSD calculations, and compare them with diffusion coefficients obtained from our mean-field approximation (MFA) given by $D(\theta) \cong (1/6)k_\theta a_\theta^2$, where k_θ and a_θ are determined from KMC simulations. The different levels of theory used to calculate diffusion coefficients are summarized in Table II. In what follows, we briefly review the KMC simulations used to calculate k_θ , a_θ , and $D(\theta)$.^{44,45}

In our calculations, we considered two simulation cell sizes, both with periodic boundary conditions: one with a single faujasite unit cell, and another containing eight faujasite unit cells. The single faujasite unit cell contains 32 S_{II} sites and 16 W sites, while eight unit cells contain 256 S_{II} sites and 128 W sites. For a given configuration, \vec{n} , of random walkers, a process list of possible hops from occupied

to empty sites is compiled for all molecules. A particular jump from site i to j is chosen from this list with a probability of $k_{i \rightarrow j}/k_{\text{tot}}(\vec{n})$, where $k_{i \rightarrow j}$ is the i to j rate coefficient calculated with the parabolic jump model, and $k_{\text{tot}}(\vec{n})$ is the sum of all rate coefficients in the process list. A hop is made every KMC step and the system clock is updated with variable time-steps.⁴⁶ The actual KMC time-step is obtained from: $\Delta t(\vec{n}) = -\ln(1-x_1)/k_{\text{tot}}(\vec{n})$, where $x_1 \in [0,1)$ is a uniform random number. In what follows, we describe the methods for calculating k_θ and a_θ for MFA, and mean square displacements for MSD (please see Table II).

The instantaneous cage-to-cage hop length, λ , and cage residence time, τ , for each individual molecule are determined as follows. First, we define the intercage jumps: if the n th location of the i th molecule is a W site during a KMC run, we calculate the distance between benzene center-of-mass positions for the previous and next jumps of this molecule, denoted steps $n-1$ and $n+1$, respectively. If this distance is nonzero and different from characteristic intracage distances,¹⁷ a cage-to-cage jump is registered with t_{n+1} and $\vec{r}_i(n+1)$ stored as the arrival time and position in the new cage, respectively. The residence time τ is the difference between t_{n+1} and the previously stored arrival time, while the intercage jump length λ is the three-dimensional norm of $\vec{r}_i(n+1)$ minus the previously stored arrival position. These quantities are averaged for each molecule over all time-steps in a KMC run to yield $k_\theta = 1/\langle \tau \rangle$ and $a_\theta^2 = \langle \lambda^2 \rangle$. A convergence criterion is that all molecules have essentially identical values of k_θ and a_θ .

We also calculate k_θ according to $k_\theta = \kappa \times k_1 \times P_1$ for comparison with $k_\theta = 1/\langle \tau \rangle$, to confirm the validity of the expression $k_\theta = \kappa \times k_1 \times P_1$. The individual quantities are determined as follows. For each molecule, $P_1 = (1 + T_2/T_1)^{-1}$, where T_1 and T_2 are the total simulation times spent in W and S_{II} sites, respectively. Furthermore, $k_1 = N^\ddagger/T_1$, where N^\ddagger is the number of visits to W sites for each molecule. Also, $\kappa = N_{\text{cc}}/N^\ddagger$, where N_{cc} is the number of cage-to-cage hops for each molecule.^{41,44} In general, the expression $k_\theta = \kappa \times k_1 \times P_1$ is found to be uniformly valid as expected.

For a given loading, we also calculate the ‘‘exact’’ self-diffusion coefficients from MSD calculations using the KMC algorithm. We obtain the MSD diffusion coefficient at a particular loading according to $D(\theta) = \lim_{t \rightarrow \infty} \langle |\vec{r}_i(t) - \vec{r}_i(0)|^2 \rangle / 6t$, where $\vec{r}_i(t)$ is the instantaneous center of mass position of molecule i at time t . The ensemble average, $\langle \dots \rangle$, averages over all time-steps *and* all molecules in the system by multiple time-step, multiple time-origin analysis of a single random walk.²² In this approach, we first choose a time bin width, Δt_{bin} , usually a fraction of the estimated mean supercage residence time. For the time $t = n\Delta t_{\text{bin}}$, the mean square displacement averaged over all molecules is given by

$$\langle \mathcal{R}^2(n\Delta t_{\text{bin}}) \rangle = \frac{1}{N} \sum_{i=1}^N \frac{1}{Q_n} \sum_{l,m} ' |\vec{r}_i(l) - \vec{r}_i(m)|^2, \quad (4.1)$$

where $\vec{r}_i(l)$ is the center-of-mass position of molecule i at KMC time t_l . The sum is restricted to those pairs (l,m) for

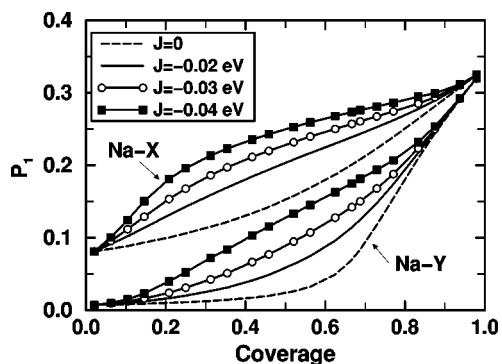


FIG. 3. P_1 from KMC as a function of θ and J , for Na-X and Na-Y at 468 K.

which $t_l - t_m$ falls into the n th time bin, characterized by $n = \text{int}[(t_l - t_m)/\Delta t_{\text{bin}}]$, and Q_n is the number of such pairs.

The loading dependence of the diffusion coefficient for a particular temperature, denoted as a ‘‘diffusion isotherm,’’¹⁰ is determined from MFA and MSD calculations by running KMC simulations at several fixed loadings. For a particular loading, convergence is obtained by requiring that all molecules give essentially identical values for k_θ and P_1 . The values of k_θ and P_1 typically vary by less than 2% after 5×10^6 Monte Carlo steps. An MSD isotherm with 21 loadings and 5×10^6 Monte Carlo steps per loading, on a single faujasite unit cell, requires 14 CPU h on an IBM RS/6000 3CT; whereas an MSD isotherm with 11 loadings and 5×10^6 Monte Carlo steps per loading, on eight unit cells, requires 44 CPU h on the same machine. MFA calculations that give diffusivities within 5% (10%) of MSD values are 5 (20) times faster than MSD calculations, respectively. These speedups should be regarded as suggestive, since their precise values depend upon numerical implementation details, which may vary among codes; the main purpose of this study is to provide the proof of principle.

V. RESULTS AND DISCUSSION

In this section, we begin by discussing the factors that comprise k_θ , namely P_1 , k_1 , and κ , to understand the loading dependence of the diffusion coefficient. Next, we compare diffusion isotherms calculated from the MFA and MSD methods (please see Table II). We then discuss the comprehensive loading and temperature dependence of benzene diffusion in faujasite. Next, we compare k_θ values from our analytical theory, MFT, to those from MFA. Finally, we compare our MSD calculated diffusion coefficients to those from pulsed-field gradient (PFG) NMR and tracer zero-length column (TZLC) data.

A. Loading dependence of P_1 , k_1 , and κ

In Fig. 3 we show the simulation results for P_1 , the probability of occupying a W site, as a function of coverage in Na-X and Na-Y at 468 K, for several values of the coupling parameter J . Figure 3 shows that P_1 increases monotonically with coverage, yielding the value 1/3 for both zeolites at full coverage. At infinite dilution, P_1 is much larger for Na-X than for Na-Y, because the W sites in Na-X are

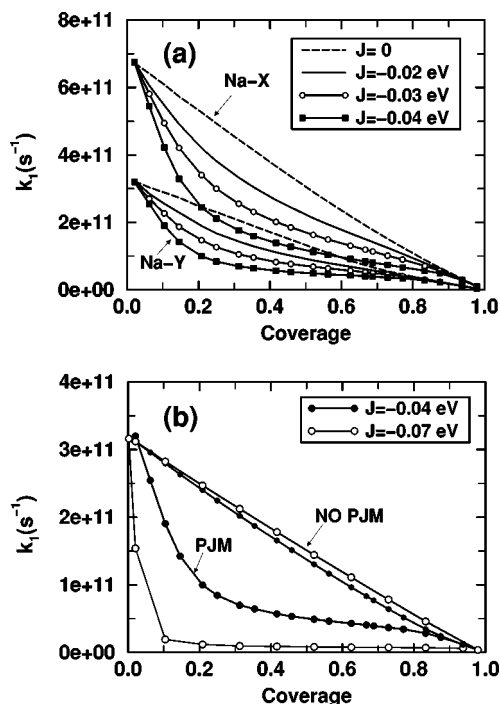


FIG. 4. (a) k_1 from KMC as a function of θ and J , for Na-X and Na-Y at 468 K; (b) k_1 from KMC with and without activation energy fluctuations modeled by the PJM.

assumed to be more stable than those in Na-Y. We also observe that the concavity of P_1 vs θ changes with different values of J . We can summarize this with the parameter $\gamma \equiv (f_1 - f_2)/|J|$, where f_1 and f_2 are the free energies for binding in W and S_{II} sites, respectively. Figure 3 shows that for both Na-X and Na-Y, P_1 is concave up with coverage when $\gamma > 3$, and is concave down when $\gamma < 3$. When γ is large, e.g., Na-Y with $J = -0.02$ eV, W sites are very unstable and fill only after most S_{II} sites are already occupied, making P_1 concave up. Alternatively, when γ is small, e.g., Na-X with $J = -0.04$ eV, W sites fill readily at low loadings, making P_1 concave down.

In Figs. 4(a) and 4(b), we show the simulation results for k_1 , the total rate of leaving a W site, as a function of coverage in Na-X and Na-Y at 468 K, for several values of the coupling parameter J . Figure 4(a) shows that k_1 decreases monotonically to zero at full coverage, as all sites become filled. At infinite dilution, we see that $k_1(X) > k_1(Y)$ because leaving the W site in Na-X is assumed to be more facile. The loading dependence of k_1 is nearly linear for $J=0$, i.e., without attractive guest-guest interactions, a result consistent with mean-field theory. The loading dependence of k_1 becomes more strongly concave up as $|J|$ increases, an important manifestation of correlations that arises from attractive interactions.

It is interesting to investigate whether the enhanced concavity of k_1 with increasing $|J|$ arises from thermodynamic or kinetic effects, i.e., from the $(1 - \theta_j)$ factors in Eq. (3.3), or from the $\langle k_{1 \rightarrow j} \rangle$ rate coefficients also in Eq. (3.3), respectively. To determine this, we calculated k_1 for Na-Y at 468 K from KMC using the PJM, and compared this to k_1 from Eq. (3.3) where θ_1 and θ_2 are obtained from the same KMC

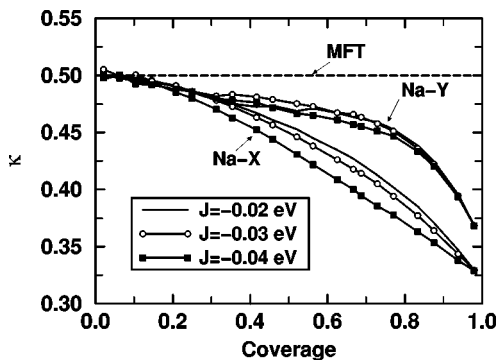


FIG. 5. κ from KMC as a function of θ and J , for Na-X and Na-Y at 468 K.

simulation, while $\langle k_{1 \rightarrow 1} \rangle$ and $\langle k_{1 \rightarrow 2} \rangle$ are replaced with their infinite dilution values. In this way, we can disentangle thermodynamic and kinetic effects that arise from guest-guest interactions. This comparison is shown in Fig. 4(b) for two values of the coupling parameter J . We see in Fig. 4(b) that without the PJM, k_1 decreases nearly linearly as if J were equal to zero, while using the PJM makes k_1 strongly concave up. The main insight gained here is that the strong correlations manifested in the curvature of k_1 vs θ arise almost exclusively from our treatment of fluctuating activation energies via the PJM.

In Fig. 5 we show the simulation results for κ , the transmission coefficient for cage-to-cage motion, as a function of coverage in Na-X and Na-Y at 468 K, for several values of the coupling parameter J . We see in Fig. 5 that the θ and J dependence of κ is relatively weak in both zeolites. The weak variation of κ indicates that the loading dependence of $k_\theta = \kappa \times k_1 \times P_1$ is predominantly controlled by k_1 and P_1 . In the next section, we will explore the accuracy of approximating the self-diffusivity according to $D(\theta) \equiv (1/6)k_\theta a_\theta^2$.

B. Loading dependence of $D(\theta)$ by MSD and MFA

In Figs. 6(a) and 6(b), we show diffusion isotherms for benzene in Na-X and Na-Y, respectively, simulated by the MSD and MFA methods at 468 K for various values of the coupling parameter J . In a previous article,¹⁰ we classified these isotherms into three different types depending on the coverage that gives the maximum diffusivity: $\theta_{\max} = 0$ is defined as type I, $\theta_{\max} \in (0, 1/2]$ is type II, and $\theta_{\max} \in (1/2, 1]$ is type III. These diffusion isotherm types can be understood as follows. When the S_{II} and W sites are nearly degenerate, the coverage dependence of P_1 is weak, and hence k_θ and $D(\theta)$ are dominated by the decreasing coverage dependence of k_1 , giving rise to a type I isotherm. Alternatively, when the sites are far from degenerate, the enhancement of P_1 at higher loadings dominates the diffusivity until $\theta_1 \sim \theta_2$, at which point the decreasing k_1 begins to dominate, giving rise to a type III isotherm. Type II isotherms arise for systems with parameters that are intermediate between type I and III. We note that our diffusion isotherm types I, II, and III correspond broadly with Kärger and Pfeifer's types I, II, and IV, respectively.²⁷

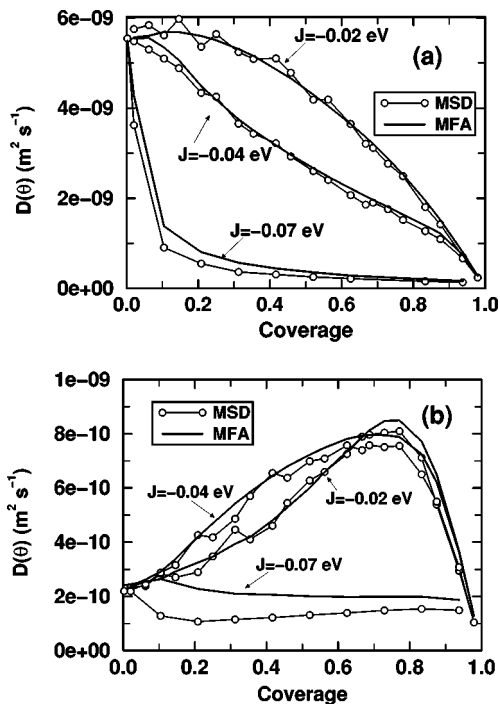


FIG. 6. Diffusion isotherms for benzene in (a) Na-X and (b) Na-Y, by MSD and MFA at 468 K for various values of J .

In Fig. 6(a), we obtain a type II isotherm for benzene in Na-X at 468 K using $J = -0.02$ eV, which goes over to a type I isotherm for $J = -0.04$ eV. When $J = -0.07$ eV, we find an interesting loading dependence, involving a sharp decrease for small loadings, followed by a broad region of constant diffusivity for higher loadings. In Fig. 6(b), we obtain a type III isotherm for benzene in Na-Y at 468 K using $J = -0.02$ eV, which remains type III for $J = -0.04$ eV. The predominance of type III for benzene in Na-Y arises because W sites in Na-Y are relatively unstable at 468 K. When $J = -0.07$ eV in Na-Y, we find another interesting loading dependence, involving a broad region of constant diffusivity for essentially all loadings. We discuss these intriguing results for $J = -0.07$ eV in Na-X and Na-Y below. In general, we find that a_θ varies very weakly with loading (data not shown), suggesting that the loading dependence of $D(\theta)$ is controlled by k_θ , and hence by k_1 and P_1 . We also find that making J more negative, while keeping all other parameters constant, changes isotherms according to type III \rightarrow II \rightarrow I.

In Figs. 6(a) and 6(b), we see excellent qualitative agreement between the MSD and MFA methods, for all values of J in both Na-X and Na-Y. This level of agreement is remarkable, considering the computational efficiency of MFA relative to MSD calculations. The percent error, calculated as $\mathcal{E} = (D_{\text{MFA}} - D_{\text{MSD}}) / D_{\text{MSD}} \times 100\%$, is shown in Figs. 7(a) and 7(b) for benzene in Na-X and Na-Y, respectively. We find that MFA diffusivities give errors comparable to statistical Monte Carlo error ($\pm 5\%$) for both zeolites with $|J| \leq 0.04$ eV and $\theta \lesssim 2/3$. This suggests that our MFA is essentially exact when some S_{II} sites are vacant. The origin of this effect becomes clear when modeling counterpermeation through anisotropic zeolite membranes.⁴⁷ The presence of

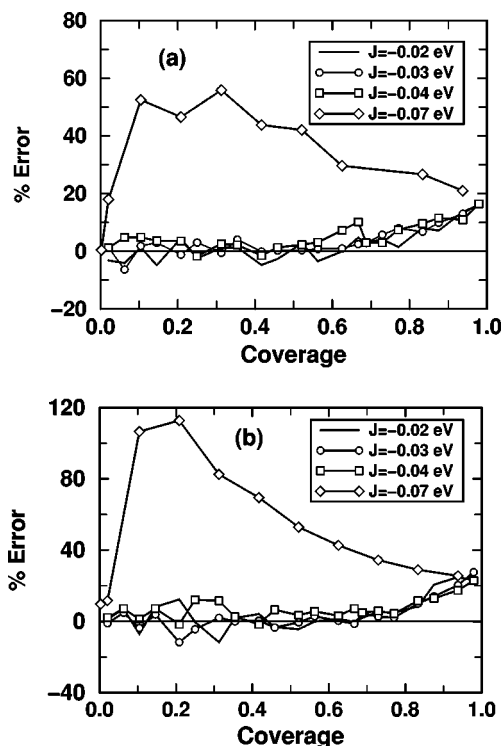


FIG. 7. Percent error between MFA and MSD diffusion coefficients for benzene in (a) Na-X and (b) Na-Y, evaluated as $(D_{\text{MFA}} - D_{\text{MSD}})/D_{\text{MSD}} \times 100\%$.

vacant S_{II} sites allows for intracage, $S_{\text{II}} \rightarrow S_{\text{II}}$ jumps, which are relatively rapid compared to intercage, $S_{\text{II}} \rightarrow W$ jumps. Although $S_{\text{II}} \rightarrow S_{\text{II}}$ jumps do not directly contribute to cage-to-cage motion, these jumps allow for rapid washing out of correlations among cage-to-cage jumps. Thus, when vacant S_{II} sites are present, rapid intracage motion gives diffusion that is accurately modeled by $D(\theta) = (1/6)k_{\theta}a_{\theta}^2$.

When most S_{II} sites are filled, correlations between $W \rightarrow W$ intercage jumps reduce diffusivities from their approximate MFA values. For coverages near full loading, MFA diffusivities give errors near 30% for all values of J , which is characteristic of the W site lattice in zeolites X and Y.⁴⁵ We have previously reported an analytical theory for these minor correlation effects,⁴⁵ and hence will not discuss them further in this article.

Figures 6(a) and 6(b) show that systems with $J = -0.07$ eV exhibit diffusivities with intriguing loading dependencies. In addition, Figs. 7(a) and 7(b) show that MFA diffusivities with $J = -0.07$ eV demonstrate very different patterns of error from those calculated with less negative values of J . Furthermore, the KMC simulations for $J = -0.07$ eV required a larger simulation cell for convergence, containing eight faujasite unit cells. These findings can be explained by considering that strongly attractive adsorbate-adsorbate interactions can induce phase transitions from low to high density of adsorbed benzene, analogous to vapor-liquid equilibrium of bulk benzene. Indeed, we have recently reported a study using grand canonical Monte Carlo and thermodynamic integration,²⁸ predicting that such phase transitions can occur for benzene in Na-X up to a critical temperature of $T_c = 370 \pm 20$ K, assuming J

$= -0.04$ eV. If we assume for the moment that $T_c \propto |J|$, then $T_c \sim 650$ K in Na-X with $J = -0.07$ eV. Since the diffusivities in Figs. 6(a) and 6(b) were calculated at 468 K, the simulations using $|J| \leq 0.04$ eV represent supercritical lattice gas diffusion, while those using $J = -0.07$ eV represent *subcritical* diffusion.

Since canonical KMC simulations fix the loading, a subcritical system at, e.g., $\theta = 0.5$ will involve a fluctuating liquidlike cluster of filled sites occupying approximately half the lattice, while a supercritical system at the same loading will be more evenly dispersed throughout the lattice. This insight explains our intriguing simulation results, and may help elucidate experimental findings as well. First, the formation of large clusters increases the system correlation length, requiring larger simulation cells for convergence. Second, cluster formation in subcritical systems suggests a diffusion mechanism involving “evaporation” of particles from clusters. Since an accurate treatment of density fluctuations at the cluster boundary is required for modeling evaporation realistically, we expect that MFA will be less accurate for subcritical systems, as shown in Figs. 7(a) and 7(b). Moreover, the distribution of cage residence times becomes multimodal for subcritical systems, making the kinetic interpretation of k_{θ} less clear. The fact that MFA still captures the qualitative loading dependencies of subcritical diffusivities, and is even correct to within a factor of ca. 2, is remarkable.

The isotherms calculated with $J = -0.07$ eV in Figs. 6(a) and 6(b) can also be understood in terms of cluster formation. Increasing the loading in subcritical systems increases mean cluster sizes, and smoothes cluster interfaces. Once these interfaces become sufficiently smooth, we can assume that evaporation dynamics remain essentially unchanged by further increases in loading. As such, we expect the subcritical diffusivity to obtain its full loading value at low loadings, and then remain roughly constant up to full loading, as shown for Na-X in Fig. 6(a). Since supercritical Na-Y systems exhibit type III isotherms in Fig. 6(b), increasing for low θ and then decreasing for high θ , we find that $D(\theta \sim 0) \cong D(\theta \sim 1)$. As a result, subcritical Na-Y systems are expected to give isotherms that are roughly constant for all loadings, as shown in Fig. 6(b).

This type of loading dependence, involving broad regions of constant diffusivity, is surprising, since isotherms for interacting adsorbates are expected to decrease with loading when site blocking dominates. It is interesting to note that an isotherm type has been reported for strongly associating adsorbates such as water and ammonia,²⁷ denoted by Kärger and Pfeifer as type III (not to be confused with our type III), involving an initial increase followed by a broad region of constant diffusivity. The present analysis suggests that Kärger and Pfeifer’s type III diffusion isotherm may be characteristic of a cluster-forming, subcritical adsorbed phase.

C. Comprehensive loading dependence of diffusion

The comprehensive loading dependence of diffusion in these systems is controlled by the degree of degeneracy between S_{II} and W sites, which depends upon three energy scales: $f_1 - f_2$, J , and $k_{\text{B}}T$. As such, two unitless parameters

TABLE III. Diffusion isotherm types as a function of χ and γ for Na–X and Na–Y.

		$\chi=(f_1-f_2)/k_B T$								$ J $ (eV) Na–X	$ J $ (eV) Na–Y
		2	3	4	5	6	7	8	9		
$\gamma=(f_1-f_2)/ J $	30	I	I	II	III	III	III	III	III	0.005	0.0085
	25	I	I	II	III	III	III	III	III	0.006	0.01
	20	I	I	II	III	III	III	III	III	0.0075	0.0125
	15	I	I	II	III	III	III	III	III	0.01	0.0167
	10	I	I	II	III	III	III	III	III	0.015	0.025
	5	I	I	II	II	III	III	III	III	0.03	0.05
	2.5	I	I	I	I	I	I	I	I	0.06	0.1
T (K)	Na–X	870	580	435	350	290	250	220	190		
T (K)	Na–Y	1450	965	725	580	480	415	360	320		

are required to describe the corresponding states of benzene in Na–X and Na–Y. In Sec. V A, we quantified the competition between host–guest and guest–guest interactions with the parameter $\gamma=(f_1-f_2)/|J|$. This parameter controls the loading dependence at low temperatures, when guest–guest interactions are required for stabilizing W sites. In a previous article,¹⁰ we discussed the parameter $\chi=(f_1-f_2)/k_B T$, which controls the loading dependence for small values of $|J|$, when thermal fluctuations are required for populating W sites.

Table III summarizes a large number of KMC simulated diffusion isotherms, calculated with various values of χ and γ . In each region of (χ, γ) -space, we performed at least two diffusion isotherm calculations using different fundamental parameter sets, e.g., one isotherm for Na–X and one for Na–Y, to confirm that these different states do indeed correspond to the same isotherm type. In Table III, we see that at low values of either χ or γ ($\chi \leq 3$, $\gamma \leq 30$) or ($\chi \leq 9$, $\gamma \leq 2.5$), where S_{II} and W sites are almost degenerate, we have a type I isotherm. Whereas at high values of either χ or γ ($\chi \geq 5$, $\gamma \geq 10$) or ($\chi \geq 6$, $\gamma \geq 5$), where S_{II} and W sites are far from degenerate, we have a type III isotherm. A type II isotherm occurs in the intermediate values of χ and γ . The boxed type II in Table III is the actual region of (χ, γ) -space that we predict represents benzene in Na–X at 468 K, while the boxed type III's model benzene in Na–Y at 468 K. In general, we see that the loading of maximum diffusivity, θ_{\max} , decreases with increasing $|J|$ and T .

D. Comparison between theory and simulation

The computational effort required to create Table III provides incentive for developing analytical theories of diffusion. In Sec. III, we described our new mean-field theory (MFT) of diffusion, which we compare with KMC in this section. Since we found in Sec. V B that $D(\theta) \cong (1/6)k_\theta a_\theta^2$, and that a_θ depends very weakly upon loading, we will compare MFT and KMC calculations of the loading and temperature dependence of k_θ . According to MFT, $k_\theta = 1/2 \times k_1 \times P_1$, where k_1 and P_1 are evaluated as described in Sec. III.

Figures 8(a) and 8(b) show k_θ for benzene in Na–X and Na–Y, respectively, calculated by MFT and KMC at 468 K for two values of the coupling parameter J . When using $J = -0.02$ eV, Figs. 8(a) and 8(b) show that MFT provides

qualitatively reasonable diffusivities, which consistently overestimate simulated values because MFT neglects correlation effects that make $\kappa < 1/2$ for finite loadings.¹⁰ Thus, we find that MFT can be used to compute diffusion isotherms for systems with low to moderate couplings.

For $J = -0.04$ eV, we find that MFT predicts phase transitions from low to high density of adsorbed benzene, analogous to vapor–liquid equilibrium of bulk benzene (cf. Sec. V B and Ref. 28). Since lattice gas MFT is implemented in the grand canonical ensemble,³⁹ phase transitions are characterized by precipitous jumps in density vs chemical potential. These jumps give rise to coexistence regions in (T, ρ) -space where equilibrium systems cannot be observed, as shown in Figs. 8(a) and 8(b) for $J = -0.04$ eV. MFT typically overestimates critical temperatures of vapor–liquid phase transitions,^{28,39} which explains why the simulated isotherms are smooth in Figs. 8(a) and 8(b), while the theoretical isotherms are not. It is interesting to note that the MFT coex-

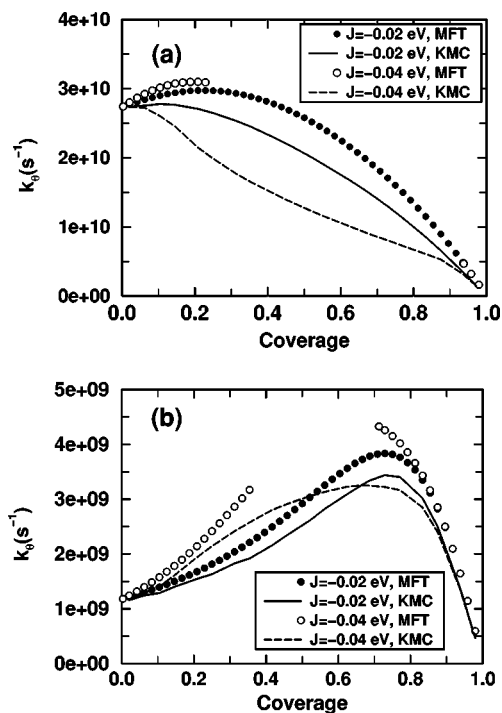


FIG. 8. Comparing k_θ from mean-field theory (MFT) and KMC at 468 K for (a) Na–X and (b) Na–Y.

TABLE IV. Apparent activation energies (eV) of k_θ for Na–X and Na–Y, calculated by MFT and KMC for different values of θ and J (eV).

Zeolite	$ J $	$\theta=0.21$		$\theta=0.94$	
		MFT	KMC	MFT	KMC
Na–X	0.02	0.202	0.208	0.134	0.125
Na–X	0.04	0.193	0.219	0.133	0.127
Na–Y	0.02	0.353	0.353	0.149	0.138
Na–Y	0.04	0.334	0.324	0.149	0.136

istence region narrows from Na–X to Na–Y, because the W site is less stable in Na–Y. As $\gamma=(f_1-f_2)/|J|$ increases, e.g., from Na–X to Na–Y, the critical temperature decreases, which narrows the coexistence region for a given temperature. As we will show in a forthcoming publication,⁴⁸ increasing γ can actually quench the phase transition, forcing the critical temperature to vanish identically.

Because of the fluctuating adsorption and activation energies in our model, it is not obvious how apparent activation energies of diffusion relate to fundamental energy scales. Although MFT was found to be only partially useful for calculating diffusion isotherms of strongly coupled systems, MFT may prove useful for predicting apparent activation energies. In Table IV, we show apparent activation energies of k_θ for Na–X and Na–Y, calculated by MFT and KMC for different values of θ and J . The results in Table IV show that MFT provides semiquantitative activation energies, which properly decrease with loading, and increase from Na–X to Na–Y. The activation energies for $\theta=0.21$ are consistently below $S_{II} \rightarrow W$ activation energies, while those for $\theta=0.94$ are consistently above $W \rightarrow W$ activation energies. We remind the reader that these conclusions are subject to the accuracy of the parabolic jump model, which will be tested in detail in a forthcoming publication.⁴⁰ Nevertheless, it is encouraging that MFT provides such an accurate description of the temperature dependence of diffusion for strongly coupled systems, at essentially no computational cost.

E. Comparison between simulation and experiment

Now that we have considered benzene in faujasite as a general model for diffusion in nanopores, we focus on benzene in Na–X using $J = -0.03$ eV, obtained from the second virial coefficient of the heat of adsorption.^{11,12} Figure 9

shows MSD calculated diffusion isotherms for benzene in Na–X at $T=393$ and 468 K, compared to PFG NMR data¹⁴ at the same temperatures (uniformly scaled by a factor of 5), and TZLC diffusivities¹⁵ at $T=468$ K (uniformly scaled by a factor of 100). The experimental data were scaled to facilitate comparison with the loading dependence predicted by simulation, which itself was *not* fitted to either experimental result. Figure 9 shows that our model is in excellent qualitative agreement with the PFG NMR results, and in qualitative disagreement with TZLC. Our model overestimates PFG NMR diffusivities at high loadings, because the lattice model allows 6 molecules per cage while the observed saturation coverage is 5.4 molecules per cage.

One way to view the discrepancy in Fig. 9, apart from the absolute magnitudes, is that both simulation and PFG NMR are consistent with a low coverage of maximum diffusivity, θ_{\max} , while TZLC exhibits a large θ_{\max} . While it is not obvious why the TZLC results differ so markedly from PFG NMR data and from our simulated diffusivities, our results in Sec. V C do suggest future experiments to test the reliability of TZLC. Indeed, we found in Sec. V C that θ_{\max} decreases with increasing temperature, as all sites become more degenerate. As such, high-temperature TZLC diffusion isotherms should be measured, to confirm consistency with our rather plausible prediction regarding the temperature dependence of θ_{\max} .

VI. SUMMARY

We have presented a lattice model of self-diffusion in nanopores, involving inhomogeneous adsorption sites, repulsive adsorbate–adsorbate interactions via site blocking, and attractive adsorbate–adsorbate interactions via the nearest-neighbor coupling parameter, J . We have developed a simple and qualitatively reliable method for describing how adsorbate–adsorbate interactions modify jump activation energies for site-to-site rate coefficients, called the parabolic jump model. We have used this model to explore the loading, temperature, and J dependence of benzene self-diffusion in Na–X and Na–Y zeolites. Our model for benzene diffusion assumes that benzene molecules jump among S_{II} and W sites, located near Na^+ ions in supercages, and in 12-ring windows separating adjacent supercages, respectively.

Various levels of theory and simulation have been proposed for calculating diffusion coefficients from our lattice model. We have implemented a variable time-step, canonical kinetic Monte Carlo (KMC) algorithm for calculating mean square displacements. We have discussed a mean-field approximation (MFA) that simplifies KMC calculations, involving diffusivities given by $D(\theta) \cong (1/6)k_\theta a_\theta^2$, where θ is the fractional loading, a_θ is the KMC calculated mean inter-cage jump length ($a_\theta \cong 11$ Å), and $1/k_\theta$ is the KMC calculated mean cage residence time. We have also derived a completely analytical, grand canonical mean-field theory (MFT) of diffusion, wherein k_θ is approximated by $k_\theta = (1/2) \times k_1 \times P_1$, where P_1 is the probability of occupying a W site, and k_1 is the total rate of leaving a W site.

We have calculated diffusion coefficients for various loadings at fixed temperature, denoted as “diffusion iso-

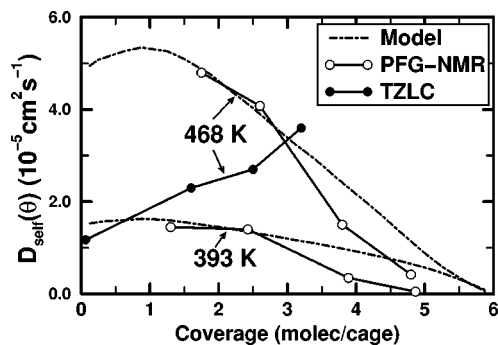


FIG. 9. Diffusion isotherm for benzene in Na–X at 468 K, by PFG NMR (scaled by 5), TZLC (scaled by 100), and by MSD simulations.

therms," with various input parameters and at various levels of theory, to determine (i) how fundamental interactions control trends in diffusion, and (ii) what levels of theory are required to treat these effects. We have found that diffusion isotherms can be segregated into subcritical and supercritical regimes, depending upon the system temperature relative to the critical temperature of the confined fluid.

Supercritical diffusion isotherms exhibit three types, depending on the coverage that gives the maximum diffusivity: $\theta_{\max}=0$ is defined as type I, $\theta_{\max}\in(0,1/2]$ is type II, and $\theta_{\max}\in(1/2,1]$ is type III. These diffusion isotherm types, which correspond broadly with Kärger and Pfeifer's types I, II, and IV, respectively,²⁷ can be understood as follows. When S_{II} and W sites are nearly degenerate, the decreasing coverage dependence of k_1 dominates and gives rise to a type I isotherm. Alternatively, when the sites are far from degenerate, the enhancement of P_1 at higher loadings gives rise to a type III isotherm. Type II arises for intermediate systems. In general, increasing $|J|$ or T , or decreasing the fundamental inhomogeneity between sites, causes the isotherms to change according to type III \rightarrow II \rightarrow I. We have discussed this finding in terms of corresponding states parameters, relating diffusion coefficients for benzene in Na-X to those in Na-Y.

Subcritical diffusion isotherms are dominated by formation of liquidlike clusters of varying sizes in the lattice. These isotherms are characterized by broad regions of constant diffusivities, since changing loading, and hence cluster size, does not qualitatively change the dynamics of evaporation from these clusters. Such subcritical diffusion isotherms may be representative of Kärger and Pfeifer's type III (not to be confused with our type III).

We have found that MFA diffusivities can describe transport semiquantitatively for a wide variety of system parameters, especially in supercritical systems where density fluctuations are more evenly dispersed throughout the lattice. Our analytical theory, MFT, provides semiquantitative apparent activation energies, and also provides qualitatively reasonable diffusion isotherms for systems at high temperatures or with low J couplings. Our model for benzene in Na-X is in excellent qualitative agreement with pulsed-field gradient NMR diffusivities, and in qualitative disagreement with tracer zero-length column (TZLC) data. We have suggested that high-temperature TZLC experiments should be performed, to test consistency with our prediction that θ_{\max} will decrease with increasing temperature.

In future work, we plan to use Chandler's transition path sampling⁴⁹ and Voter's accelerated molecular dynamics⁵⁰ to test predictions from our parabolic jump model. We also plan to apply this flavor of diffusion theory to other host-guest lattices, and to nonequilibrium systems under various forms of flow. Finally, we plan to explore the parameter dependence of vapor-liquid equilibrium in nanopores, and to study further the relationship between phase transitions and diffusion in nanopores.

ACKNOWLEDGMENTS

The authors thank Dr. Peter H. Nelson and Dr. Fabien Jousse for stimulating discussions. S.M.A. thanks the Na-

tional Science Foundation Grant Nos. (CHE-9616019 and CTS-9734153) for generous funding. C.S. thanks UMass Amherst for a 1998-1999 Graduate School Fellowship.

- ¹J. Kärger and D. M. Ruthven, *Diffusion in Zeolites and Other Microporous Solids* (Wiley, New York, 1992).
- ²N. Y. Chen, T. F. Degnan, Jr., and C. M. Smith, *Molecular Transport and Reaction in Zeolites* (VCH, New York, 1994).
- ³K. Hahn, J. Kärger, and V. Kukla, *Phys. Rev. Lett.* **76**, 2762 (1996).
- ⁴V. Gupta, S. S. Nivarthi, D. Keffer, A. V. McCormick, and H. T. Davis, *Science* **274**, 164 (1996).
- ⁵D. S. Sholl and K. A. Fichthorn, *Phys. Rev. Lett.* **79**, 3569 (1997).
- ⁶C. Saravanan and S. M. Auerbach, *J. Chem. Phys.* **107**, 8120 (1997).
- ⁷D. E. Favre, D. J. Schaefer, S. M. Auerbach, and B. F. Chmelka, *Phys. Rev. Lett.* **81**, 5852 (1998).
- ⁸D. Keffer, A. V. McCormick, and H. T. Davis, *J. Phys. Chem.* **100**, 967 (1996).
- ⁹C. Rodenbeck, J. Kärger, and K. Hahn, *Phys. Rev. E* **55**, 5697 (1997).
- ¹⁰C. Saravanan, F. Jousse, and S. M. Auerbach, *Phys. Rev. Lett.* **80**, 5754 (1998).
- ¹¹D. Barthomeuf and B. H. Ha, *J. Chem. Soc., Faraday Trans.* **69**, 2147 (1973).
- ¹²D. Barthomeuf and B. H. Ha, *J. Chem. Soc., Faraday Trans.* **69**, 2158 (1973).
- ¹³O. M. Dzhigit, A. V. Kiselev, and T. A. Rachmanova, *Zeolites* **4**, 389 (1984).
- ¹⁴A. Germanus, J. Kärger, H. Pfeifer, N. N. Samulevic, and S. P. Zdanov, *Zeolites* **5**, 91 (1985).
- ¹⁵S. Brandani, Z. Xu, and D. Ruthven, *Microporous Mater.* **7**, 323 (1996).
- ¹⁶J. Kärger and D. M. Ruthven, *Stud. Surf. Sci. Catal.* **105**, 1843 (1997).
- ¹⁷A. N. Fitch, H. Jobic, and A. Renouprez, *J. Phys. Chem.* **90**, 1311 (1986).
- ¹⁸G. Vitale, C. F. Mellot, L. M. Bull, and A. K. Cheetham, *J. Phys. Chem. B* **101**, 4559 (1997).
- ¹⁹P. Demontis, S. Yashonath, and M. L. Klein, *J. Phys. Chem.* **93**, 5016 (1989).
- ²⁰L. M. Bull, N. J. Henson, A. K. Cheetham, J. M. Newsam, and S. J. Heyes, *J. Phys. Chem.* **97**, 11776 (1993).
- ²¹P. J. O'Malley and C. J. Braithwaite, *Zeolites* **15**, 198 (1995).
- ²²S. M. Auerbach, N. J. Henson, A. K. Cheetham, and H. I. Metiu, *J. Phys. Chem.* **99**, 10600 (1995).
- ²³S. M. Auerbach, L. M. Bull, N. J. Henson, H. I. Metiu, and A. K. Cheetham, *J. Phys. Chem.* **100**, 5923 (1996).
- ²⁴T. Mosell, G. Schrimpf, and J. Brickmann, *J. Phys. Chem. B* **101**, 9476 (1997).
- ²⁵T. Mosell, G. Schrimpf, and J. Brickmann, *J. Phys. Chem. B* **101**, 9485 (1997).
- ²⁶F. Jousse and S. M. Auerbach, *J. Chem. Phys.* **107**, 9629 (1997).
- ²⁷J. Kärger and H. Pfeifer, *Zeolites* **7**, 90 (1987).
- ²⁸C. Saravanan and S. M. Auerbach, *J. Chem. Phys.* **109**, 8755 (1998).
- ²⁹T. Hjelt, I. Vattulainen, J. Merikoski, T. Ala-Nissila, and S. C. Ying, *Surf. Sci.* **380**, 501 (1997).
- ³⁰M. O. Coppens, A. T. Bell, and A. K. Chakraborty, *Chem. Eng. Sci.* **53**, 2053 (1998).
- ³¹F. Jousse, S. M. Auerbach, and D. P. Vercauteren, *J. Phys. Chem. B* **102**, 6507 (1998).
- ³²R. L. June, A. T. Bell, and D. N. Theodorou, *J. Phys. Chem.* **95**, 8866 (1991).
- ³³M. Wilhelm, A. Firouzi, D. E. Favre, L. M. Bull, D. J. Schaefer, and B. F. Chmelka, *J. Am. Chem. Soc.* **117**, 2923 (1995).
- ³⁴D. J. Schaefer, D. E. Favre, M. Wilhelm, S. J. Weigel, and B. F. Chmelka, *J. Am. Chem. Soc.* **119**, 9252 (1997).
- ³⁵D. H. Olson, *Zeolites* **15**, 439 (1995).
- ³⁶H. Jobic, personal communication, 1998.
- ³⁷H. Klein, H. Fuess, and G. Schrimpf, *J. Phys. Chem.* **100**, 11101 (1996).
- ³⁸E. S. Hood, B. H. Toby, and W. H. Weinberg, *Phys. Rev. Lett.* **55**, 2437 (1985).
- ³⁹D. Chandler, *Introduction to Modern Statistical Mechanics* (Oxford University Press, New York, 1987).
- ⁴⁰F. Jousse and S. M. Auerbach, in preparation, 1998.
- ⁴¹S. M. Auerbach, *J. Chem. Phys.* **106**, 7810 (1997).
- ⁴²S. M. Auerbach and H. I. Metiu, *J. Chem. Phys.* **105**, 3753 (1996).
- ⁴³W. H. Press, S. A. Teukolsky, W. T. Vetterling, and B. P. Flannery,

- Numerical Recipes in Fortran* (Cambridge University Press, New York, 1992).
- ⁴⁴C. Saravanan and S. M. Auerbach, J. Chem. Phys. **107**, 8132 (1997).
- ⁴⁵C. Saravanan, F. Jousse, and S. M. Auerbach, J. Chem. Phys. **108**, 2162 (1998).
- ⁴⁶P. Maksym, Semicond. Sci. Technol. **3**, 594 (1988).
- ⁴⁷P. H. Nelson and S. M. Auerbach, invited by Chem. Eng. J. (1999), in press.
- ⁴⁸I. Dukovski, C. Saravanan, S. M. Auerbach, and J. Machta, in preparation, 1999.
- ⁴⁹C. Dellago, P. G. Bolhuis, F. S. Csajka, and D. Chandler, J. Chem. Phys. **108**, 1964 (1998).
- ⁵⁰A. Voter, J. Chem. Phys. **106**, 4665 (1997).